Ag–SiO2 Core–Shell Nanorod Arrays: Morphological, Optical, SERS, and Wetting Properties

ARTICLE *in* LANGMUIR · DECEMBER 2011

Impact Factor: 4.46 · DOI: 10.1021/la203772u · Source: PubMed

5 AUTHORS, INCLUDING:

Jun Chen
Georgia Institute of Technology
51 PUBLICATIONS **1,444** CITATIONS
SEE PROFILE

Justin L Abell
University of Georgia
21 PUBLICATIONS **228** CITATIONS
SEE PROFILE

Langmuir

Article

pubs.acs.org/Langmuir

Ag−SiO_2 Core−Shell Nanorod Arrays: Morphological, Optical, SERS, and Wetting Properties

Chunyuan Song,[†,‡] Jun Chen,[§] Justin L. Abell,[§] Yiping Cui,*[,‡] and Yiping Zhao*[,†]

Nanoscale Science and Engineering Center, [†]Department of Physics and Astronomy, and [§]Department of Biological and Agricultural Engineering, The University of Georgia, Athens, Georgia 30602, United States

[‡]Advanced Photonics Center, Southeast University, Nanjing 210096, P.R. China

Supporting Information

ABSTRACT: Using the hydrolysis of tetraethylorthosilicate, a uniform and conformal layer of porous SiO_2 with controlled thickness has been coated onto the oblique angle deposited Ag nanorod (AgNR) array to form an aligned AgNR-SiO_2 core−shell array nanostructure. The morphology, optical property, SERS response, and surface wettability of the AgNRs with different SiO_2 shell thicknesses have been obtained by multiple characterization techniques. The morphological characterization shows that each AgNR on the array is coated with a uniform and porous silica shell independently and the growth of shell thickness follows a linear function versus the coating time. Thickening of the shell induces a monotonic decrease of the apparent contact angle, red-shift of the transverse mode of the localized surface plasmon resonance peak, and makes the SiO_2 shell more compact. The SERS response of 4-Mercaptophenol on these substrates exhibits an exponential decay behavior with the increasing coating time, which is ascribed to the decreasing Ag surface coverage of core−shell nanorods. Under the assumption that the Ag surface coverage is proportional to the SERS intensity, one can estimate the evolution of SiO_2 coverage on AgNRs. Such coverage evolution can be used to qualitatively explain the LSPR wavelength change and quantitatively interpret the contact angle change based on a double Cassie's law.

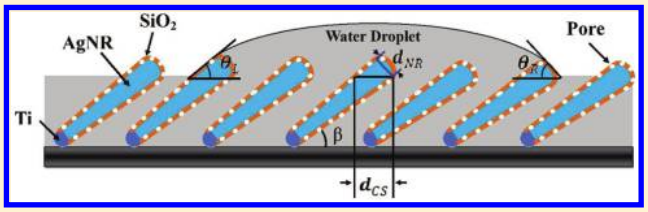

1. INTRODUCTION

Surface-enhanced Raman scattering (SERS) provides a powerful means of obtaining vibrational fingerprint information on adsorbates with ultrahigh sensitivity and excellent frequency resolution. This technique has recently received considerable attention in surface science, electrochemistry, analytical chemistry, biological, and biomedical research.[1−5] So far, a wide range of SERS studies have aimed at investigating structure, topology, and composition of biochemical species. The most critical aspect of performing these SERS applications is the fabrication of SERS-active substrates with large SERS enhancement, high sensitivity, fine uniformity, good reproducibility, and biocompatibility.[6,7]

A novel aligned silver nanorod (AgNR) array, fabricated by oblique angle deposition (OAD) method, has been verified as an extremely sensitive, reproducible, and uniform substrate for SERS detection.[8−12] The SERS enhancement factor of the AgNR array is $>10^8$, and the signal collected on multiple spots on the same substrate and from different batches of substrates show small relative standard deviation (RSD) of 10% and 15%, respectively.[13] Using this substrate, different chemical and biological agents have been successfully detected.[11,13−15] However, since the aligned AgNR array is deposited by physical means, and exposed directly to the ambient environment without any safeguard, many issues have been revealed with regard to the SERS application of this substrate, such as surface contamination, stability, and biocompatibility.[16] The excellent optical properties can readily deteriorate when the substrate is exposed to air or other chemicals such as acids or halides. Furthermore, silver surface is not a desirable biocompatible interface for biological sample immobilization.[16] To overcome these shortcomings, some modifications to this substrate have been proposed. One of the potential solutions is to replace silver with gold, since gold is known as a biocompatible SERS-active material with more stable physical and chemical properties. While this has been successfully done by OAD method in our lab (unpublished) clearly this is a very expensive process and not feasible for practical application. Besides, we have also coated the as-deposited AgNR with gold by galvanic replacement reaction and the characterization results confirmed that the resulted Au-modified AgNR array shows good SERS enhancement ability with improved stability and high sensitivity of air contamination detection.[17] Compared with the gold modification, another simple and inexpensive approach is to coat the AgNR with a layer of SiO_2. Silica has demonstrated as a wonderful coating material to enhance the stability of nanoparticles, provide tunable solubility in various solvents, or even tailor their size and shape-dependent optical properties.[18−21] Another advantage of silica is its robust surface chemical properties, which can be achieved through chemical

Received: September 27, 2011
Revised: November 7, 2011
Published: December 12, 2011

bonding with a large variety of available silane coupling agents. These versatile surfaces can serve as a platform for the conjugation of biomolecules or chemical materials, and has opened up a wide range of new opportunities in biomedical applications as sensors, markers, and probes.[22,23] So far, the SiO_2-coated Ag colloids showing desirable physical and chemical properties have been successfully used in metal-enhanced fluorescence,[24] SERS-based protein detection,[25,26] drug release,[27] antibacterial application,[28,29] to name a few. These Ag-SiO_2 core−shell structures have also been used for studying some special physical and chemical mechanisms. For example, Wang and Xu mixed Ag-core SiO_2-shell colloids with R6G and placed this suspension in a sealed quartz cell for probing spatial distribution of electromagnetic (EM) field enhancement via SERS.[30] Lacy and his co-workers soaked a SiO_2-coated silver-island film substrate in to a reporter solution contained cuvette, and preformed an in situ SERS investigation for adsorption kinetic studies.[31] In these experiments, the SERS substrates were immersed in the analyte solutions to monitor the spatial distribution of EM field or molecular absorption kinetics.

In this paper, we investigate the use of OAD-generated AgNR arrays as a template to fabricate aligned AgNR-core SiO_2-shell arrays with controlled shell thicknesses via hydrolysis of tetraethylorthosilicate (TEOS). The resulting morphological, optical, SERS, and wetting properties are studied systematically by transmission electron microscope, UV−vis absorbance spectroscopy, and contact angle measurement. Since 4-mercaptophenol molecules selectively adsorb to Ag surface rather than SiO_2, SERS response of 4-mercaptophenol can be used to characterize the surface coverage of SiO_2 on the template. The characterization results show that the growth of the SiO_2 shell follows a linear trend as a function of the coating time. Along with the shell growth, the localized surface plasmon resonance (LSPR) peak red-shifts monotonically. Continuous coating of SiO_2 on the AgNR surface makes the shell more compact, which gradually decrease the area of the immobilized Raman reporters on the substrate. The changes of surface wettability and SERS signal induced by SiO_2 coating are consistent with each other through a double Cassie's model.

2. EXPERIMENTAL SECTION

2.1. Chemicals. Tetraethylorthosilicate (TEOS, 99.9%) and citrate acid (99%) were obtained from Alfa Aesar. Ammonium hydroxide (28.0−30.0 wt.%) was purchased from J. T. Baker. Ethanol (EtOH, 95%) and 4-mercaptophenol (MPh, 97%) were acquired from Aldrich. All of the reagents were used without further purification. Silver (99.999%) and titanium (99.995%) were purchased from Kurt J. Lesker as evaporation source. Deionized (DI) water was used in all reactions.

2.2. AgNR Array Deposition. The AgNR arrays used in this study were fabricated by the OAD method using a custom-designed electron-beam evaporation system.[8,13,32] In brief, glass slides (Fisherbrand and Gold Seal, cutting into 9 mm ×9 mm) were cleaned by Piranha solution (4:1 v/v H_2SO_4:H_2O_2) for 30 min followed by DI water rinsing and nitrogen (N_2) blow-drying, and were served as the substrates for deposition. The substrates were positioned in the vacuum chamber so that the vapor incident direction was at an angle $\theta = 0°$ or 86° with respect to the surface normal of the substrates for Ag film or AgNRs deposition, respectively. During the evaporation, a quartz crystal microbalance (QCM) directly facing the vapor was used to monitor both the thickness and the rate of the deposition. Ti was used as an adhesion layer and was deposited at $\theta = 0°$ or 86° for Ag film or AgNR depositions, respectively, to a QCM thickness of 20 nm at a rate of 0.2 nm/s. For Ag film and AgNR fabrication the Ag deposition rate was set at 0.3 nm/s. For all depositions, the chamber pressure was below 3×10^{-6} Torr.

2.3. AgNR−SiO_2 Core−Shell Nanostructure Fabrications. The silica shell growth with desired thickness on the AgNRs were realized by silanization via hydrolysis of TEOS.[33] Briefly, 12 pieces of as-prepared AgNR arrays were first soaked into 0.5 M citric acid for 30 min to clean surface contaminations and modify the surface with citric groups. After rinsing with DI water and blow-drying with N_2, the arrays were immerged into a homogeneous mixture composed of 30 mL of EtOH, 4 mL of H_2O, and 500 μL of TEOS for 20 min under stirring. Once 560 μL of ammonium hydroxide was added into the mixture, the reaction was initiated. The shell thickness was controlled by the hydrolysis time of TEOS after the accession of alkaline. The AgNR arrays were removed from the reaction solution after a series of determined reaction time t, t = 5, 10, 15, 20, 25, 30, 35, 40, 50, 60, 90, and 120 min, followed by water rinsing and N_2 drying. All samples were stored in a vacuum chamber for further characterization.

2.4. Instrumentation. The optical extinction spectra of the samples were collected by a JASCO (Easton, MD) V-570 UV/vis/NIR double beam spectrophotometer with a clean glass slide as the reference. The morphology of the as-deposited AgNR array was characterized by a field-emission scanning electron microscope (FE-SEM; FEI, Inspect F). To obtain the SiO_2 shell growth process on isolated AgNRs, the SiO_2-coated AgNRs with different coating time were dispersed into ethanol by an ultrasonic bath and then transferred onto Cu grids for transmission electron microscope (TEM; FEI, Tecnai 20) characterization. For SERS measurements, the AgNR-SiO_2 core−shell samples were soaked in 1 mL of 1 mM MPh aqueous solution for 30 min followed by water rinsing. After drying by N_2, the SERS spectra of MPh were acquired by a HRC-10HT Raman analyzer (Enwave Optronics Inc.), with a laser beam of 785 nm excitation wavelength, 30 mW output power, ∼100 μm laser spot diameter, and a collection time of 5 s. The contact angles of the as-deposited AgNR array, SiO_2-coated AgNR samples, and Ag film were measured by the sessile drop method (Data Physics OCA 20) with a 2 μL water droplet within 10 min after their removal from the vacuum storage chamber.

3. RESULTS AND DISCUSSION

3.1. Morphological Evolutions. Figure 1 shows the SEM image of an as-deposited AgNR array (t = 0 min). The surface is composed of tilted, randomly distributed, aligned AgNRs with a wide range of morphologies, such as corrugations, bifurcations, protrusions, as well as random irregularities. The nanorod density is $\eta = 11.3 \pm 0.6$ rods/μm^2. The average diameter of the AgNRs (top) is $d_{NR} \approx 100$ nm and the length is approximated as ∼1000 nm with tilted angle $\beta \approx 70°$. This is the typical AgNR structure we obtained from the OAD deposition.[13,32] A representative TEM image of the as-deposited AgNRs is shown in Figure 2a. The surface of the AgNRs is relatively smooth and the selective area electron diffraction pattern (the image inserted in Figure 2a) demonstrates the polycrystalline nature of the AgNRs. To compare with the as-deposited AgNR without SiO_2 shells, Figure 2b−f shows the representative TEM images of AgNRs

dx.doi.org/10.1021/la203772u | Langmuir 2012, 28, 1488−1495

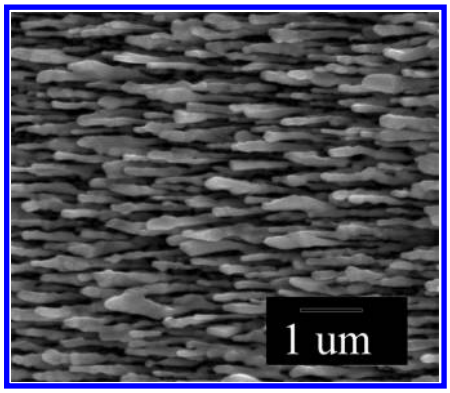

Figure 1. SEM image of the as-deposited AgNR array fabricated by OAD method at 86°.

coated with SiO_2 for t = 5, 10, 20, 40, and 60 min, respectively. After the hydrolysis of TEOS on the AgNR array for 5 min, an ultrathin layer of SiO_2 (thickness d = 1.9 ± 0.4 nm) is conformally coated onto the AgNR template. As the reaction continued, the thickness of the SiO_2 shell increases from d = 2.2 ± 0.3 nm at t = 10 min to d = 16 ± 1 nm at t = 60 min, as shown in Figure 2c–f. The growth thickness of the shell is plotted in Figure 3. The fitting result shows that the d–t curve follows a linear relationship, $d = \gamma t$, where γ = 0.274 ± 0.005 nm/min and the goodness of fit R^2 = 0.998. Furthermore, as shown in the TEM images, at the beginning of the coating ($t \leq$ 10 min), the ultrathin SiO_2 layer on the AgNR appears noncompact with an ambiguous boundary. When the shell grows to 6.0 ± 0.7 nm at t = 20 min, a visible boundary of the SiO_2 layer is found in Figure 2d. As the reaction proceeded for 40 min, a thicker shell (d = 11 ± 1 nm) is built on the AgNR template, and some visible particles interspersed on the shell as the dark spots appear in Figure 2e. With further reaction, as shown in Figure 2f (t = 60 min), the surface of the shell is occupied by a number of bigger particles (diameter ~5 nm), resulting in a relatively rough coating surface. According to the reaction mechanism, the silver template might be attacked by the ammonium hydroxid and result in $Ag(NH_3)_2^+$, forming $[Ag(NH_3)_2]OH$ during the coating process. If these particles

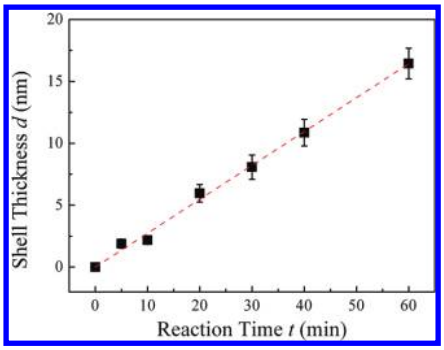

Figure 3. Average thickness d of the SiO_2 shell versus of the reaction time t, d = 0.274t.

are insoluble $[Ag(NH_3)_2]OH$, such a significant etching should also be found from the morphological change of the AgNRs, i.e., some Ag on the top of the AgNR should be etched and leave behind some hollows enclosed by well-controlled silica wall (same as the phenomenon reported by Yin[34]). In fact, we cannot find any hollow structures on the surface of the AgNR (Figure 2f). Thus, the etching of silver is not significant enough to be observed until the coating has processed for a long reaction time.[34] The almost unchanged AgNR morphology indicates that the Ag template might only be etched very slightly in the ammonium hydroxide solution during the 60 min reaction. Moreover, during the coating process the suspended SiO_2 nanoparticles are also synthesized in the reaction medium. It is possible that some very small SiO_2 nuclei are formed (invisible in the TEM image) at the early stage of the reaction, and these nuclei grow bigger with time and deposit onto the SiO_2 shell as seen in Figure 2f, which is consistent with the growth trend of the particles shown in TEM images. On the basis of above experimental results and analysis, we can claim that a number of particles absorbed on silica surface are some individual silica nanoparticles rather than the $[Ag(NH_3)_2]OH$.

Many published works have confirmed that the SiO_2 shell synthesized by the Stöber process is composed of porous amorphous silica.[35−37] On the basis of aforementioned morphological observations, we can conceive the growth process of the porous SiO_2 shell on the AgNRs.[34,38] At the

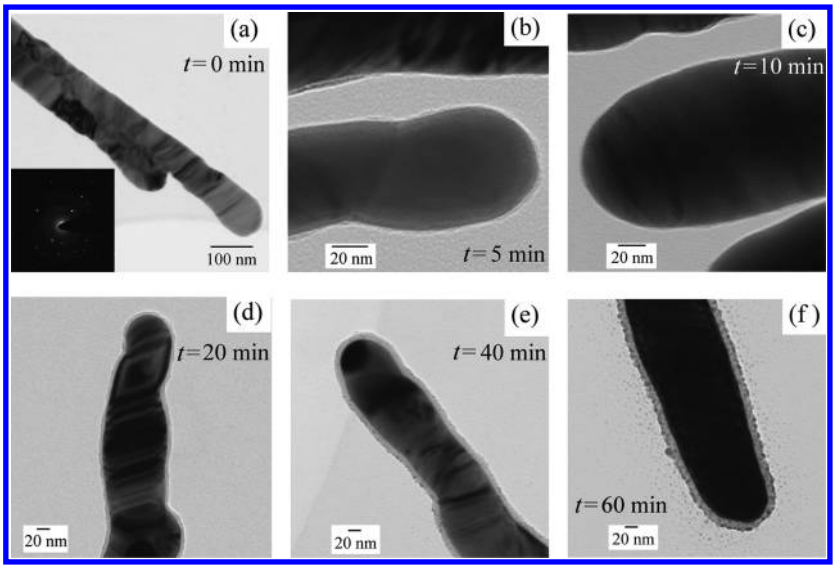

Figure 2. TEM images of the NR samples before and after coating with a layer of SiO_2 for different reaction times.

dx.doi.org/10.1021/la203772u | Langmuir 2012, 28, 1488–1495

very early stage of the coating, SiO_2 islands nucleate randomly on the AgNR templates with the nanometer scale pores. These islands grow bigger (both in diameter and thickness) and connect together with subsequent SiO_2 deposition. As a result, the surface coverage of SiO_2 on the AgNR increases and the porosity of the SiO_2 shell as well as the pore size decrease. Regardless of the random morphology and/or polycrystalline nature of the AgNRs, the SiO_2 coating appears extremely uniform and conformal, demonstrating that the coating process is independent of these factors.

3.2. Wettability. The wettability of SiO_2-coated AgNRs has been characterized using a water contact angle measurement. Since the nanorods are tilted with respect to surface normal, it is expected that the contract angles parallel and antiparallel to the tilting direction are different as illustrated in Figure 4. We

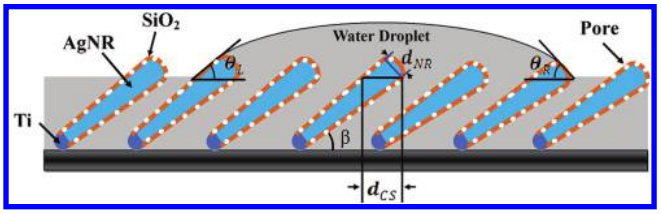

Figure 4. Schematic diagram of the water droplet on SiO_2-coated AgNRs. Image not drawn to scale.

denote the contract angle measured along the rod titling direction as θ_L, and opposite direction is θ_R. Figure 5a plots the

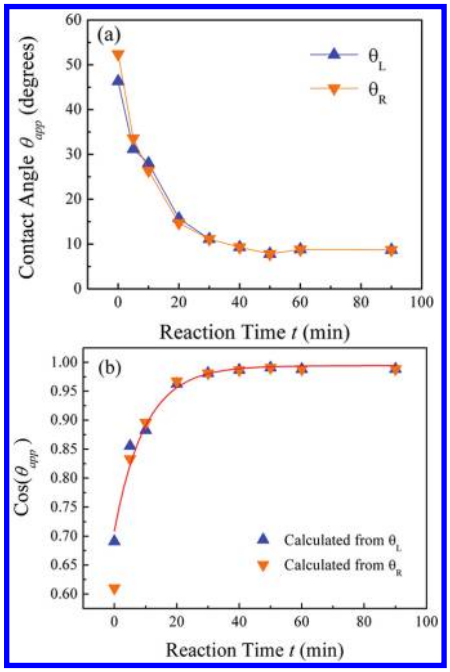

Figure 5. (a) Comparison of contact angles at both edges of the droplet measured on the AgNR substrates coated by SiO_2 for different reaction time t and (b) the cosine values of these angles and the fitting results of double Cassie's Model with fixed $f_{Ag}(t)$.

contact angles θ_L and θ_R versus the reaction time t (scattered symbols). Both the θ_L and θ_R decrease monotonically with t. For the as-deposited AgNRs substrate, θ_R = 52.4° and θ_L = 46.3°, and $\Delta\theta = \theta_R - \theta_L$ = 6.1°. Such a difference is owing to the anisotropic nature of the tilted AgNRs. With the increase of SiO_2 coverage, the $\Delta\theta$ becomes smaller. For example, for t = 5 min, θ_R = 33.6° and θ_L = 31.2°, and $\Delta\theta$ = 2.4°. For t = 60 min, θ_R = 8.8° and θ_L = 8.8°, and $\Delta\theta$ = 0. This result implies that with more SiO_2 coverage, the nanorod surface becomes more hydrophilic. The contact angle difference caused by the titled NR morphology is compromised by the hydrophilic surface; that is, the morphological effect on the contact angle becomes less significant when the surface becomes more hydrophilic.

3.3. Extinction Property. The UV−vis optical extinction properties of these silica shell coated AgNR array is shown in Figure 6. The optical extinction spectrum of the as-deposited

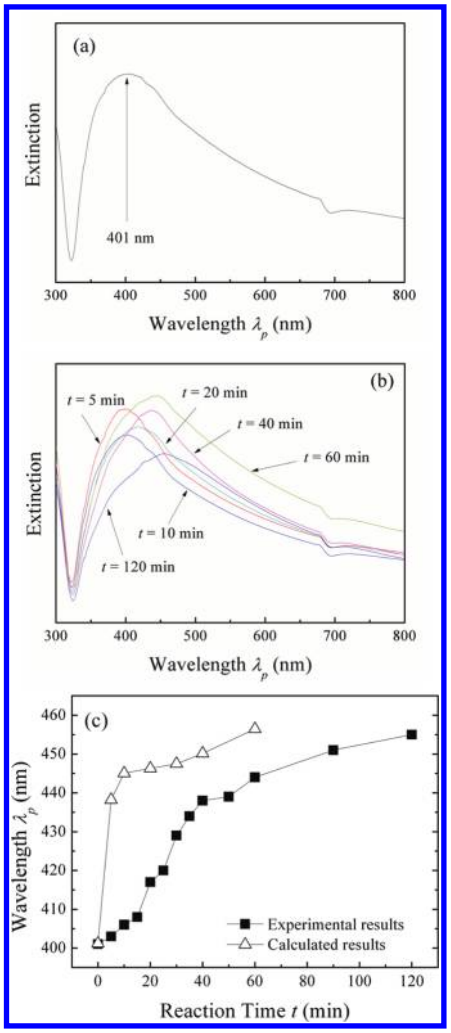

Figure 6. (a) LSPR feature of the as-deposited AgNR array, (b) the LSPR spectra of the AgNR array coated by SiO_2 for different reaction time, and (c) the comparison of experimentally and theoretically determined λ_p by the Maxwell−Garnett formula and eq 1.

AgNR array (Figure 6a) shows a strong extinction peak at λ_p = 401 nm. This peak corresponds to the transverse mode (TM) LSPR of the AgNRs, and the longitudinal mode (LM) is located in the infrared region which cannot be observed with the instrument we used.[39] Figure 6b plots the extinction spectra of the SiO_2-coated AgNR samples prepared for reaction time t = 5, 10, 20, 40, 60, and 120 min, respectively. With the increase of the reaction time, the TM LSPR peak red-shifts monotonically as a result of the growth of the SiO_2 shell. For example, a ~1.9 nm ultrathin SiO_2 shell (t = 5 min) results in the TM LSPR peak λ_p shifting slightly to 403 nm. After 60 min coating (d = 16 ± 1 nm), the λ_p red-shifts to 444 nm and finally reaches

dx.doi.org/10.1021/la203772u | Langmuir 2012, 28, 1488−1495

to 455 nm when the SiO_2 coating is stopped at t = 120 min. The summarized λ_p–t relationship is plotted in Figure 6c. These observations are consistent with the previous reports that coating metal nanoparticles with silica causes a significant red-shift in the corresponding LSPR, which can be explained by the change of the refractive index surrounding the AgNR.[40]

3.4. SERS Response. The SERS response of the AgNR-core SiO_2-shell arrays with different shell thicknesses are tested using MPh as a reporter which has very weak adhesion on SiO_2 surface but can strongly adsorb to Ag surfaces via S–Ag covalent bond.[41] According to a previous study, the MPh forms a self-assembled monolayer on Ag. The typical SERS spectrum of MPh measured on the as-deposited AgNR substrate is shown in Figure 7a. The characteristic peak at $\Delta\nu$ = 1079 cm^{-1} is the

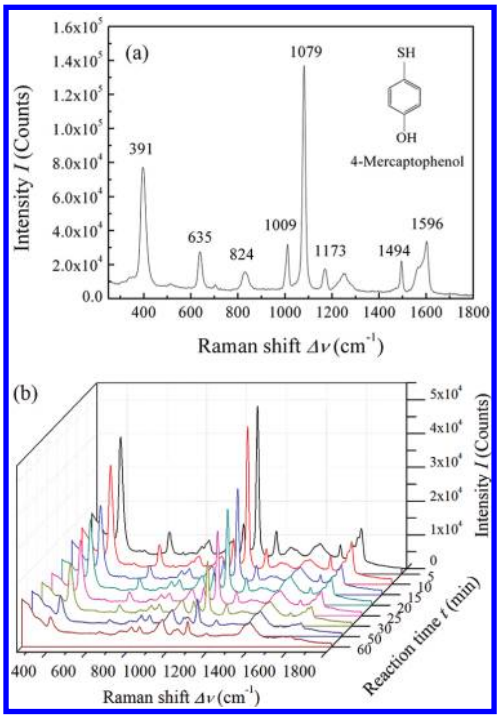

Figure 7. (a) SERS spectrum of MPh on the as-deposited AgNR assay substrate and (b) the SiO_2-coated AgNR substrates for different reaction times t.

ring breathing mode ν_1 (Wilson notation) and the other peaks at $\Delta\nu_1$ = 391, 635, 824, 1009, 1173, 1494, and 1596 cm^{-1} correspond to the ring mode vibration of 7a, 12a, 6a, 18a, 9a, 19a, and 8a, respectively.[41] These SERS peaks with high signal-to-noise ratio demonstrate that the as-deposited AgNR array has a very high enhancement factor (EF) (our previous work demonstrates that the EF > 10^8).[13] Figure 7b shows the SERS spectra of MPh obtained on AgNR-core SiO_2-shell substrates with the coating time t = 5, 10, 15, 20, 25, 30, 50, and 60 min, respectively. Note that besides the normal MPh Raman peaks, two additional SERS peaks at $\Delta\nu$ = 949 and 1394 cm^{-1} appear as shown in Figure 7b. They can be assigned to the characteristic Raman peaks of citrate. Figure S1 shows the comparison of SERS spectra of the AgNR substrates treated by four different methods, as-deposited, treated with citrate, after hydrolysis, and after MPh immersion. The black curve shows the background of the as-deposited AgNR substrate. After being treated with citrate acid, a distinct SERS signal of citrate is detected on the substrate (red curve). The following SiO_2 shell coating for t = 5 min results in the SERS signal of citrate decreasing slightly (blue curve). After soaking in MPh, the cyan curve demonstrates that most of the citrate groups on the substrate are replaced by MPh and the residual signal of citrate does not pose a threat to the intensity characterization at $\Delta\nu$ = 1079 cm^{-1}. With increasing t, the SERS intensity of the MPh at $\Delta\nu$ = 1079 cm^{-1} (I_{1079}) decreases monotonically. The intensity drops to one-third, from I_{1079} = 129 000 ± 800 counts at t = 0 min to I_{1079} = 39 000 ± 900 counts when a ~2.2 nm thick SiO_2 shell is grown at t = 10 min. When the SiO_2 shell grows to ~6 nm at t = 20 min, the SERS signal decreases to I_{1079} = 21 000 ± 2000 counts. After coating SiO_2 for t = 60 min, only a very weak SERS signal of MPh (I_{1079} = 2300 ± 200 counts) can be detected. The normalized SERS intensity $I_{1079}(t)/I_{1079}(0)$ is plotted as a function of time in Figure 8.

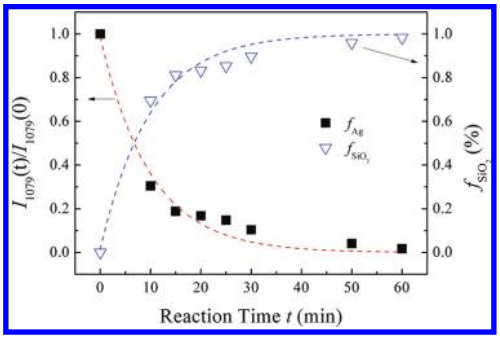

Figure 8. SERS intensity ratio $I_{1079}(t)/I_{1079}(0)$ and SiO_2 surface coverage $f_{SiO_2}(t)$ as a function of SiO_2 coating time t.

3.5. Discussion. The observed SERS performance, LSPR peak shift, and the wetting behavior are closely related to the porous silica layer growth as shown in Figure 2, especially the coverage and porosity of silica on AgNRs. Thus, the reaction time-dependent relations of SERS (Figure 7), LSPR peak (Figure 6), and contact angle (Figure 5) are closely related. Although the TEM images in Figure 2 clearly demonstrate the conformal coating of the silica layer, obtaining the coverage and porosity information directly is challenging. Thus the underlying connection between SERS, LSPR and contract angle measurements must be ascertained.

According to the current SERS theory,[42] the SERS enhancement results from enhanced localized electromagnetic field (EM enhancement), as well as the chemical enhancement (CE) via charge transfer (CT) between the analyte molecules and metallic surface. One of the key differences between EM and CE is that the CT is strictly limited to molecules in direct contact with the metal surface,[43] while the EM effect is distance dependent and the enhancement region has been predicted to attenuate rapidly within a few nanometers away from the metal surfaces. Using small spherical Ag nanoparticle (NP) as an example, the theoretical overall distance dependence of the EM enhancement is $1/r^{12}$,[43] where r is the distance of the molecule from the surface. The SiO_2 layer therefore results in a physical and chemical barrier separating the analyte from metal surface, which can block the charge transfer and establish a very thin SERS active layer around the AgNRs. In our experiment, all of the AgNR-core SiO_2-shell substrates are each soaked in 1 mL of 1 mM MPh aqueous solution for 30 min, and then removed from the solution followed with thorough rinsing. Such a treatment results in a maximum SERS intensity at 1079 cm^{-1} (prolonged treatment such as t = 60 min gives similar SERS

dx.doi.org/10.1021/la203772u | Langmuir 2012, 28, 1488–1495

intensity as shown in Figure S2), indicates that the 30 min soaking time is enough for MPh to diffuse to the surface of AgNR and reach chemical equilibrium. Since the adsorption of MPh molecules on SiO_2 surface is very weak, while MPh can strongly bind to Ag surface, and considering the distance dependence of SERS effect, after thorough wash, we can assume that only the molecules selectively immobilized on the Ag surface remain on the substrate and the few residual molecules capped in the porous SiO_2 can be ignored. From our previous study, we have found that the enhancement is mainly from the side wall of the AgNRs, and the enhancement factor strongly depends on the length and density of the nanorods.[44] Since the shape and density of the AgNRs in this study do not change, we can assume that the enhancement factor does not change, and the SERS intensity only relates to the amounts of MPh absorbed on the AgNR surface. Note that in this core–shell structure, the coating layer of SiO_2 is very thin (~1.9 nm (t = 5 min) to ~16 nm (t = 60 min)), the shell layer will not attenuate SERS signal significantly. Thus, the resulting SERS intensity can be assumed to be proportional to the number of MPh molecules adsorbed on Ag surface, and the observed decrease in SERS intensity with respect to reaction time could be explained primarily by the decrease in the number of MPh molecules adsorbed on the silver.

Assuming that MPh molecules are only adsorbed on the exposed Ag surface as a monolayer, and the SERS enhancement factor at the Ag surface is a constant,[8,32] the resulting SERS intensity of MPh can be related to the exposed Ag area

$$I_{1079}(t) \propto N(t) \tag{1}$$

where $I_{1079}(t)$ is the measured SERS intensity at $\Delta\nu$ = 1079 cm^{-1} on the AgNR–SiO_2 core–shell SERS substrate with different coating time t and $N(t)$ is the number of MPh molecules immobilized on the substrates. Since MPh forms a monolayer on Ag, $N(t)$ is expected to be proportional to the exposed AgNR surface area $\sigma(t)$

$$N(t) \propto \sigma(t) \tag{2}$$

Combining eqs 1 and 2, one can directly relate $I_{1079}(t)$ to $\sigma(t)$ by

$$I_{1079}(t) \propto \sigma(t) \tag{3}$$

Though the SEM image (Figure 1) shows that the aligned AgNRs are in a wide range of morphologies, our previous works demonstrated that the SERS response of this substrate was very uniform.[11,13] This is due to the statistic nature of the measurement. For the measurements such as extinction, SERS and contact angle, the sampling dimension is in the scale of micrometer to millimeter. For example, for SERS detection, the diameter of laser spot is ~100 μm, in such an area, there are ~88 000 nanorods in the spot. The sampling areas for extinction and contact angle measurements are even bigger. Therefore, in all the measurements, statistically the surface of the SERS substrate is uniform, and the fraction of exposed silver surface on the AgNR, $f_{Ag}(t)$, can be estimated as

$$f_{Ag}(t) = \frac{\sigma(t)}{\sigma(0)} = \frac{I_{1079}(t)}{I_{1079}(0)} \tag{4}$$

where $\sigma(0)$ is the total surface area of AgNRs on the as-deposited AgNR array and $I_{1079}(0)$ is the SERS intensity at these conditions. Thus, the plot of $I_{1079}(t)/I_{1079}(0)$ versus t in Figure 8 represents the Ag coverage on the AgNR surface. We find that the ultrathin shell formed in the first 10 min covers approximately 70% surface area of the AgNR, and f_{Ag} = 30% of Ag surface is available to adsorb the analyte. At t = 60 min, $f_{Ag} \approx$ 1.7%, which indicate that an almost completely compact shell with few pore is formed. The f_{Ag}–t relationship can be fit with an exponential decay function, $f_{Ag}(t) = f_{Ag0}\exp(-t/k)$, as shown by the dashed red curve in Figure 8, where f_{Ag0} = 0.99 ± 0.05 and k = 9.9 ± 0.8 min^{-1}. Once $f_{Ag}(t)$ is calculated, the surface coverage fraction of SiO_2 on AgNR, $f_{SiO_2}(t)$, can be estimated as

$$f_{SiO_2}(t) = 1 - f_{Ag}(t) = 1 - f_{Ag0}\exp(-t/k) \tag{5}$$

The f_{SiO_2}–t is also plotted in Figure 8 (open triangles). The estimated coverage $f_{SiO_2}(t)$ can be used to predict reaction time-dependent behaviors of LSPR peak λ_p and contact angle θ.

The shift of the LSPR peak λ_p is caused by the change of index of refraction surrounding the AgNRs. The effect of the surrounding medium on the plasmon resonance wavelength of spherical NPs can be approximatively described as[45]

$$\lambda_p = \lambda_{p,b}(2n_0^2 + 1)^{1/2} \approx 3^{1/2}\lambda_{p,b}\left\{1 + \frac{1}{3}[n_0 - 1]\right\} \tag{6}$$

where λ_p is the particle plasmon wavelength, $\lambda_{p,b}$ is the bulk plasmon wavelength, and n_0 is the index of refraction of the surrounding medium. After coating a porous layer of SiO_2 on the Ag nanoparticle, the surrounding medium can be considered as a combination of SiO_2 and air. According to the effective medium theory, the Maxwell-Garnett formula,[46] the effective medium of this composite layer, ε_{eff}, can be estimated from $(\varepsilon_{eff} - \varepsilon_{air})/(\varepsilon_{eff} - 2\varepsilon_{air}) = f_{SiO_2}(\varepsilon_{SiO_2} - 1)/(\varepsilon_{SiO_2} + 2)$, where $\varepsilon_{air} \approx 1$ is the dielectric constant of air, ε_{SiO_2} is the dielectric constant of SiO_2, and f_{SiO_2} is the volume fraction of SiO_2 which increases with the continuous SiO_2 coating. The increasing f_{SiO_2} (Figure 8) results in an increasing ε_{eff} which demonstrates an increasing n_0. Using f_{SiO_2} derived from eq 5 and the dielectric constant of nanoporous SiO_2 synthesized by TEOS hydrolysis $\varepsilon_{SiO_2} \approx 2$,[47] we plot the predicated λ_p shift according to eq 6 as a function of coating time in Figure 6(c) (open triangles). Note that we normalized λ_p at t = 0 min using the λ_p value of the as-deposited AgNRs. The predicted results do not agree well with the experimental data but the general trends are agreeable. This discrepancy could be due to the fact that equation eq 6 is derived for spherical particles while experimental data are obtained from AgNRs. For both the calculated results of the spherical NP and the experimental data of AgNR, λ_p demonstrates a rapid red-shift when the SiO_2 coating is thin. After a thicker coating, the change of λ_p becomes slow and almost saturated.

The evolution of contact angle also results from the increasing SiO_2 coating coverage on the AgNR templates. For the AgNR–SiO_2 core–shell structure, the surface is not only geometrically rough (composed of tilted, randomly distributed AgNR with a wide range of morphologies, as shown in Figure 2) but also chemically heterogeneous (a composite surface of Ag and SiO_2). We can model the wetting behavior of such a nanostructure with a double Cassie's law. Assuming that the AgNR surface is composed with uniform and heterogeneous Ag and SiO_2, the apparent contact angle θ^* of such a heterogeneous flat surface is determined by the classical

dx.doi.org/10.1021/la203772u | Langmuir 2012, 28, 1488–1495

Cassie's law[48]

$$\cos\theta^* = f_{Ag}(t)\cos\theta_{Ag} + [1 - f_{Ag}(t)]\cos\theta_{SiO_2} \quad (7)$$

where θ_{Ag} and θ_{SiO_2} are the contact angle of the water droplet on flat Ag and silica surfaces, respectively. For the AgNR array structure, as illustrated in Figure 4 and demonstrated by the experiments, the effect of anisotropic morphology on the contact angle will be dominated by the hydrophilicity. Therefore, we can model the measured contact angles of the AgNR surface as isotropic porous layer. According to Quere,[49] because the measured contact angles of those NR surfaces are small (<60°), some liquid can escape from the deposited water droplet and instantaneously penetrate into the gap between nanorods, as indicated in Figure 4. The droplet could find itself essentially on a wet surface viewed as patches of water on SiO_2-coated AgNRs. Consequently, the experimentally measured contact angle θ_{app} is the result of the composite water−Ag/SiO_2 core−shell surface. We can apply the classic Cassie's law again to obtain θ_{app}

$$\cos\theta_{app} = f_{H_2O} + (1 - f_{H_2O})\cos\theta^* \quad (8)$$

where θ^* is determined by eq 7 and f_{H_2O} is the surface area fraction occupied by water for the NR structure and can be estimated from SEM (Figure1). Combining eqs 7 and 8, we can find that θ_{app} is a function of t

$$\cos\theta_{app}(t) = f_{H_2O} + (1 - f_{H_2O})\{f_{Ag}(t)\cos\theta_{Ag} + [1 - f_{Ag}(t)]\cos\theta_{SiO_2}\} \quad (9)$$

The f_{Ag}−t relationship is given by eq 4 though the SERS measurement. Therefore, we can fit the contact angles plotted in Figure 5a using eq 9. Figure 5b shows the fitting result (red curve) for $\cos\theta_{app} - t$, with the fitting parameters as f_{H_2O} = 0.62, $\cos\theta_{Ag}$ = 0.22 (θ_{Ag} = 77.2°), and $\cos\theta_{SiO_2}$ = 0.98 (θ_{SiO_2} = 10.1°). According to Figures 1 and 4, and because the AgNRs are tilted, we can estimate f_{H_2O}, as $f_{H_2O} = 1 - \pi d_{cs}^2\eta$ = 0.64, where d_{cs} is the effective diameter of the cross section enclosed by water as shown in Figure 4. This value is close to the fitting value 0.62. The measured contact angle of a flat Ag film, θ_{Ag} = 79 ± 1°, which is also consistent with the fitting result of θ_{Ag} = 77.2°. The reported contact angle of the silica surface fabricated by TEOS hydrolysis is 10°.[50] We find good agreement between of the measured parameters f_{H_2O}, θ_{Ag}, and θ_{SiO_2} with the fitting data confirming that our assumptions of MPh on AgNR are reasonable, and the double Cassie's law can be applied to predict the wettability properties of heterogeneous Ag-SiO_2 nanorod arrays or similar structures. Thus, the SERS, LSPR and wetting properties of the SiO_2-coated AgNR are indeed all intimately related.

4. CONCLUSION

We have demonstrated a rapid, straightforward, and inexpensive means to controllably coat a uniform layer of amorphous SiO_2 on OAD-generated AgNR arrays via hydrolysis of TEOS. The morphology, optical properties, SERS response, and surface wettability of the aligned SiO_2-coated AgNR samples have been characterized by TEM, UV/vis spectrophotometer, Raman spectroscopy, and contact angle measurement, respectively. Based on the multiple characterizations, the properties of the AgNR-core SiO_2-shell arrays are studied systematically. The TEM images indicate that the thickness of silica shell can be conveniently controlled by changing the coating time and the thickness grows following a linear function with the reaction time. The resulting SiO_2 shell is very uniform and independent of the morphology of the AgNR template. The growth of SiO_2 not only makes the porous shell more compact, but also induces a monotonic decrease of apparent contact angle and red-shift of the TM LSPR peak of the AgNR. The corresponding SERS intensity shows an exponential decay using MPh as a probe. The SERS intensity is primarily determined by the adsorbed amount of probe molecules adsorbed onto the AgNRs by which the surface coverage of SiO_2 on the AgNR template can be calculated, and used to predict the LSPR peak shift and apparent contact angle change of the SiO_2−AgNR surface versus reaction time. A double Cassie's law is proposed to predict the contact angle of the heterogeneous aligned nanorod array. Our results demonstrate that it is possible to use the simple hydrolysis process to modify the AgNR surface and change its SERS and wetting properties.

■ ASSOCIATED CONTENT

Supporting Information

SERS response of the AgNR substrate with different treatments (Figure S1). Comparison of the SERS intensity at 1079 cm^{-1} detected on the SiO_2-coated AgNR substrates (Figure S2). This material is available free of charge via the Internet at http://pubs.acs.org.

■ AUTHOR INFORMATION

Corresponding Author

*E-mail: zhaoy@uga.edu; cyp@seu.edu.cn.

■ ACKNOWLEDGMENTS

C.Y.S. and Y.P.Z are supported by National Science Foundation under contract number ECCS-1029609. J.L.A. thanks the support from USDA CSREES Grant No. 2009-35603-05001. C.Y.S. and Y.P.C. are grateful to China Scholarship Council and the Scientific Research Foundation of Graduate School of Southeast University (No. YBJJ0924) for their financial support. The authors thank Dr. Jianguo Fan and Jing Chen for their help in this work.

■ REFERENCES

(1) Kang, T.; Yoo, S. M.; Yoon, I.; Lee, S. Y.; Kim, B. *Nano Lett.* **2010**, *10*, 1189−1193.
(2) Roguska, A.; Kudelski, A.; Pisarek, M.; Lewandowska, M.; Kurzydlowski, K. J.; Janik-Czachor, M. *Surf. Sci.* **2009**, *603*, 2820−2824.
(3) Song, C. Y.; Wang, Z. Y.; Zhang, R. H.; Yang, J.; Tan, X. B.; Cui, Y. P. *Biosens. Bioelectron.* **2009**, *25*, 826−831.
(4) Ambrosio, R. C.; Gewirth, A. A. *Anal. Chem.* **2010**, *82*, 1305−1310.
(5) Doering, W. E.; Piotti, M. E.; Natan, M. J.; Freeman, R. G. *Adv. Mater.* **2007**, *19*, 3100−3108.
(6) Schatz, G. C.; Young, M. A.; Van Duyne, R. P. *Top Appl. Phys.* **2006**, *103*, 19−45.
(7) Norrod, K. L.; Sudnik, L. M.; Rousell, D.; Rowlen, K. L. *Appl. Spectrosc.* **1997**, *51*, 994−1001.
(8) Chaney, S. B.; Shanmukh, S.; Dluhy, R. A.; Zhao, Y. P. *Appl. Phys. Lett.* **2005**, *87*, 031908.
(9) Tripp, R. A.; Dluhy, R. A.; Zhao, Y. P. *Nano Today* **2008**, *3*, 31−37.

(10) Driskell, J. D.; Zhu, Y.; Kirkwood, C. D.; Zhao, Y. P.; Dluhy, R. A.; Tripp, R. A. *Plos One* **2010**, *5*, e10222.
(11) Abell, J. L.; Driskell, J. D.; Dluhy, R. A.; Tripp, R. A.; Zhao, Y. P. *Biosens. Bioelectron.* **2009**, *24*, 3663−3670.
(12) Wachter, E. A.; Moore, A. K.; Haas, J. W. *Vib. Spectrosc.* **1992**, *3*, 73−78.
(13) Driskell, J. D.; Shanmukh, S.; Liu, Y.; Chaney, S. B.; Tang, X. J.; Zhao, Y. P.; Dluhy, R. A. *J. Phys. Chem. C* **2008**, *112*, 895−901.
(14) Shanmukh, S.; Jones, L.; Driskell, J.; Zhao, Y. P.; Dluhy, R.; Tripp, R. A. *Nano Lett.* **2006**, *6*, 2630−2636.
(15) Chu, H. Y.; Huang, Y. W.; Zhao, Y. P. *Appl. Spectrosc.* **2008**, *62*, 922−931.
(16) Kim, N. H.; Lee, S. J.; Kim, K. *Chem. Commun.* **2003**, *6*, 724−725.
(17) Song, C. Y.; Abell, L. J.; He Y. P.; Murph, H. S.; Cui, Y. P.; Zhao Y. P. *J. Mater. Chem.* **2012**, DOI:10.1039/C1JM14133C.
(18) Ow, H.; Larson, D. R.; Srivastava, M.; Baird, B. A.; Webb, W. W.; Wiesner, U. *Nano Lett.* **2005**, *5*, 113−117.
(19) Wang, J.; White, W. B.; Adair, J. H. *Mater. Sci. Eng.: B* **2010**, *166*, 235−238.
(20) Tan, X.; Wang, Z.; Wang, H.; Yang, J.; Li, J.; Song, C.; Zhang, R.; Cui, Y. *Chin. Opt. Lett.* **2010**, *8*, 357−360.
(21) Hunyadi, S. E.; Murphy, C. J. *Abstr. Paper Am. Chem. Soc.* **2005**, *230*, U1159.
(22) Rocks, L.; Faulds, K.; Graham, D. *Chem. Commun.* **2011**, *47*, 4415−4417.
(23) Gong, J. L.; Jiang, J. H.; Liang, Y.; Shen, G. L.; Yu, R. Q. *J. Colloid Interface Sci.* **2006**, *298*, 752−756.
(24) Aslan, K.; Wu, M.; Lakowicz, J. R.; Geddes, C. D. *J. Am. Chem. Soc.* **2007**, *129*, 1524−1525.
(25) Chen, L.; Han, X.; Yang, J.; Zhou, J.; Song, W.; Zhao, B.; Xu, W.; Ozaki, Y. *J. Colloid Interface Sci.* **2011**, *360*, 482−487.
(26) Gong, J. L.; Liang, Y.; Huang, Y.; Chen, J. W.; Jiang, J. H.; Shen, G. L.; Yu, R. Q. *Biosens. Bioelectron.* **2007**, *22*, 1501−1507.
(27) Le, Y.; Hou, P.; Wang, J.; Chen, J. F. *Mater. Chem. Phys.* **2010**, *120*, 351−355.
(28) Xu, K.; Wang, J. X.; Kang, X. L.; Chen, J. F. *Mater. Lett.* **2009**, *63*, 31−33.
(29) Fuertes, G.; Sanchez-Munoz, O. L.; Pedrueza, E.; Abderrafi, K.; Salgado, J.; Jimenez, E. *Langmuir* **2011**, *27*, 2826−2833.
(30) Wang, W.; Li, Z.; Gu, B.; Zhang, Z.; Xu, H. *ACS Nano* **2009**, *3*, 3493−3496.
(31) Lacy, W. B.; Williams, J. M.; Wenzler, L. A.; Beebe, T. P.; Harris, J. M. *Anal. Chem.* **1996**, *68*, 1003−1011.
(32) Liu, Y. J.; Chu, H. Y.; Zhao, Y. P. *J. Phys. Chem. C* **2010**, *114*, 8176−8183.
(33) Stober, W.; Fink, A.; Bohn, E. *J. Colloid Interface Sci.* **1968**, *26*, 62−69.
(34) Yin, Y. D.; Lu, Y.; Sun, Y. G.; Xia, Y. N. *Nano Lett.* **2002**, *2*, 427−430.
(35) Walcarius, A.; Despas, C.; Bessiere, J. *Microporous Mesoporous Mater.* **1998**, *23*, 309−313.
(36) Lu, Y.; McLellan, J.; Xia, Y. N. *Langmuir* **2004**, *20*, 3464−3470.
(37) Nikolić, M.; Giannakopoulos, K. P.; Srdić, V. V. *Process. Appl. Ceram.* **2010**, *4*, 81−85.
(38) Lu, Y.; Yin, Y. D.; Li, Z. Y.; Xia, Y. N. *Nano Lett.* **2002**, *2*, 785−788.
(39) Zhao, Y. P.; Chaney, S. B.; Zhang, Z. Y. *J. Appl. Phys.* **2006**, *100*, 063527.
(40) Rodriguez-Fernandez, J.; Pastoriza-Santos, I.; Perez-Juste, J.; de Abajo, F. J. G.; Liz-Marzan, L. M. *J. Phys. Chem. C* **2007**, *111*, 13361−13366.
(41) Lee, H. M.; Kim, M. S.; Kim, K. *Vib. Spectrosc.* **1994**, *6*, 205−214.
(42) Otto, A.; Futamata, M. *Surf. Enhanced Raman Scattering* **2006**, 147−182.
(43) Kennedy, B. J.; Spaeth, S.; Dickey, M.; Carron, K. T. *J. Phys. Chem. B* **1999**, *103*, 3640−3646.
(44) Liu, Y. J.; Zhang, Z. Y.; Zhao, Q.; Dluhy, R. A.; Zhao, Y. P. *J. Phys. Chem. C* **2009**, *113*, 9664−9669.
(45) Kelly, K. L.; Coronado, E.; Zhao, L. L.; Schatz, G. C. *J. Phys. Chem. B* **2003**, *107*, 668−677.
(46) Choy, T. C. *International series of monographs on physics 1999*; Oxford University Press: New York, 1999.
(47) Yin, M.; Yao, X.; Wu, X. *Chin. J. Mater. Res.* **2003**, *17*, 220−224.
(48) Cassie, A.; Baxter, S. *Trans. Faraday Soc.* **1944**, *40*, 546−551.
(49) Bico, J.; Tordeux, C.; Quere, D. *EPL* **2001**, *55*, 214−220.
(50) Latthe, S. S.; Imai, H.; Ganesan, V.; Venkateswara Rao, A. *Microporous Mesoporous Mater.* **2010**, *130*, 115−121.